

1 **Sub-daily signals in GPS observations and their effect at semi-annual and annual**
2 **periods**

3

4 Matt A. King

5 School of Civil Engineering and Geosciences, Newcastle University, Newcastle upon
6 Tyne, NE1 7RU, United Kingdom

7 E: m.a.king@ncl.ac.uk; P: +44 (0)191 222 7833; F: +44 (0)191 222 6502

8

9 Christopher S. Watson

10 Centre for Spatial Information Science, School of Geography and Environmental Studies,
11 University of Tasmania, Private Bag 76, Hobart, Tasmania, 7001, Australia

12

13 Nigel T. Penna, Peter J. Clarke

14 School of Civil Engineering and Geosciences, Newcastle University, Newcastle upon
15 Tyne, NE1 7RU, United Kingdom

16

17 **Abstract:** Estimates of seasonal geophysical loading from GPS may be biased by
18 propagated unmodeled sub-daily signals. Although the major geophysical signals at semi-
19 diurnal and diurnal frequencies are now routinely modeled in GPS analyses, the
20 characteristics of unmodeled or mismodeled sub-daily signals are not well known. Here,
21 using site coordinates estimated every 5 minutes, we examine the sub-daily coordinate
22 spectral characteristics for ~90 global GPS sites. Unmodeled signals with amplitudes at
23 the 10 mm level are present at frequencies between ~1/day and the Nyquist frequency.
24 These are shown to propagate into 24 h solutions with (among other frequencies) annual

25 and semi-annual periods with amplitudes up to 5 mm, with a median amplitude in the
26 height component of 0.8 mm (annual) and 0.6 mm (semi-annual). They are shown to bias
27 low-degree spherical harmonics estimates of geophysical loading at the level of 5-10%,
28 although the exact effect will be network dependent.

An edited version of this paper was published by AGU. Copyright (2008) American Geophysical Union.

King, M. A., C. S. Watson, N. T. Penna, and P. J. Clarke (2008), Subdaily signals in GPS observations and their effect at semiannual and annual periods, *Geophys. Res. Lett.*, 35, L03302, doi:10.1029/2007GL032252.

29 **1. Introduction**

30 Geodetic measurements of periodic deformations of the Earth at annual and semi-annual
31 timescales provide important information on the global water cycle [*Blewitt et al.*, 2001;
32 *Mangiarotti et al.*, 2001; *van Dam and Wahr*, 1998; *Wu et al.*, 2003]. GPS measurements
33 are of particular importance due to the spatial density and distribution of the global GPS
34 network [*Wu et al.*, 2003]. However, GPS estimates of long (semi-annual to annual)
35 period surface deformations are not currently in close agreement with independent
36 GRACE estimates, for example [*King et al.*, 2006; *van Dam et al.*, 2007]. Of particular
37 relevance is the effect of propagation of unmodeled or mis-modeled sub-daily GPS
38 signals into annual, semi-annual and other long-period signals [*Penna and Stewart*, 2003;
39 *Stewart et al.*, 2005], sometimes occurring with admittances of greater than 100% [*Penna*
40 *et al.*, 2007]. For example, using conventional precise point positioning (PPP) techniques
41 with data from International GNSS Service (IGS; [*Dow et al.*, 2005]) site KARR (21°S,
42 117°E), *Penna et al.* [2007] showed that an unmodeled signal of 3.4 mm amplitude with
43 period 12 h (S2) in the north component propagates into a 4.2 mm amplitude semi-annual
44 signal in the height component, an admittance of >120%. The accurate estimation of
45 deformation (normally of the order of a few mm) at seasonal timescales using GPS
46 therefore requires a rigorous treatment of sub-daily geophysical and non-geophysical
47 systematic error sources.

48

49 Sub-daily periodic signals affecting GPS observations may originate from relatively well-
50 known phenomena such as solid Earth tides, ocean tide loading, atmospheric pressure
51 loading and higher-order ionospheric delays. Other sub-daily effects include inadequate
52 satellite orbit modeling, tropospheric mapping function errors and multipath (see also *Ray*

53 *et al.* [2007]). However, only solid Earth tide and ocean tide loading displacements are
54 currently routinely modeled at the observation level in GPS data analyses and given the
55 potential impact of the aforementioned admittances, errors in the modeling of all sub-
56 daily phenomena must be considered (see *Watson et al.* [2006] for an example dealing
57 with two disparate solid Earth tide models). The spectral characteristics of the unmodeled
58 signal sources are sparsely understood [*Fritsche et al.*, 2005; *Tregoning and van Dam*,
59 2005] and we note that sub-daily signals have been identified in Earth orientation
60 parameters [*Rothacher et al.*, 2001], tropospheric zenith delay estimates [*Humphreys et*
61 *al.*, 2005] and coordinate time series [*Khan and Scherneck*, 2003] derived from GPS
62 observations. In each of these cases the sub-daily spectrum has only been partially
63 explained and the influence of these signals on standard 24 h GPS coordinate time series
64 is not yet known.

65

66 To better understand the range and distribution of signals at sub-daily periods influencing
67 GPS analyses, we examine the frequency content of sub-daily coordinate time series for
68 ~90 globally distributed GPS sites. Through the simultaneous analysis of conventional
69 24 h GPS solutions we also investigate and quantify the propagation of these high-
70 frequency signals into spurious low-frequency signals at annual and semi-annual periods.

71

72 **2. Method and data**

73 We analyzed GPS data collected between 2000.0 and 2006.0 at 90 of the IGS IGb00
74 reference sites (Figure 1) using the PPP strategy in GIPSY/OASIS v4 [Zumberge *et al.*,
75 1997]. In contrast to conventional positioning analyses, we estimate site coordinates every
76 5 minutes, refining a strategy previously used to measure ocean tides [King and Aoki,
77 2003] and ocean tide loading displacements [King, 2006]. First, the pseudorange data for
78 each site session are smoothed using the carrier phase and then both the pseudorange and
79 carrier data are decimated to 5 minute intervals. Next, the Jet Propulsion Laboratory (JPL)
80 fiducial satellite orbits, clocks and Earth orientation parameters are held fixed, while
81 station coordinates and tropospheric zenith delays are estimated at each epoch as random
82 walk parameters and receiver clocks as a white noise process. Random walk process noise
83 was set at 60 mm/ \sqrt{h} and 4.8 mm/ \sqrt{h} for the coordinates and tropospheric parameters
84 respectively. A range of coordinate process noise values were tested with little difference
85 found in the amplitude of the dominant sub-daily spectrum. The selected value is loose
86 [King and Aoki, 2003] in order to avoid any possibility of over-smoothing the time series.
87 Ambiguities were not fixed to integers. Solid Earth tides and ocean tide loading
88 displacements were modeled according to IERS2003 standards [McCarthy and Petit,
89 2004] and the TPXO6.2 ocean tide model convolved through Green's functions
90 respectively [Egbert and Erofeeva, 2002; Agnew, 1997]. To reduce day boundary jumps,
91 data were processed in 30 h batches and then subsequently windowed to span a single
92 24 h period covering one UT day.

93

94 We note that using a simplified GPS model for site coordinates estimated every 24 h, the
95 work of Stewart *et al.* [2005] predicts the existence of spurious low frequency signals in

96 coordinate time series as a result of unmodeled periodic signals at diurnal and semi-
97 diurnal frequencies. The same theory allows for spurious signals to be present even when
98 coordinates are generated at high rates, such as in our 5 minute solutions, since the effect
99 of the repeat period of the satellite constellation remains. To examine this, Eq. 30 of
100 *Stewart et al.* [2005] was evaluated for the major tidal constituents for a period of ten
101 years. Analysis of the resultant time series spectra suggests that in addition to the real
102 input signal, spurious sub-daily signals may exist in our time series at sub-daily
103 frequencies, but with amplitudes three orders of magnitude smaller than the real signal.
104 No long-period spurious signals were predicted using the 5 minute solutions. These
105 results were confirmed using a realistic GPS simulator [*King et al.*, 2003]. Since these
106 effects are small, the high-frequency component of our 5 minute solution coordinate time
107 series is expected to be influenced most significantly by unmodeled or mismodeled
108 signals as previously discussed. The low-frequency component of the 5 minute solution
109 spectra is, however, expected to be free from spurious propagated signals.
110
111 To compare with these solutions, we repeated the GPS data analysis except that site
112 coordinates were estimated every 24 h and using only data in that window (i.e.,
113 conventional 24 h GPS PPP analyses with ambiguities not fixed to integers). Otherwise,
114 the solutions were identical to those from which the sub-daily signals were estimated,
115 including the modeling of ocean tide loading displacements and solid Earth tides.

116 **3. Coordinate time series analysis**

117 **3.1 Sub-daily spectra**

118 We computed the coordinate time series amplitude spectra, using the approach of *Scargle*
119 [1982] as described in *Press et al.* [1992], after sub-sampling to one coordinate per 0.5 h
120 and removing outliers defined by a tolerance of ± 4 times the inter-quartile range. Typical
121 high-frequency spectra for the three coordinate components are shown for site GOLD in
122 Figure 2. Signals are evident and observed at all sites at or near several major tidal
123 frequencies, such as K1, K2, S1, S2, but also at other frequencies including the harmonics
124 of K1. The spectra show some site-to-site and component-to-component variability with
125 respect to relative signal magnitude and the exact period of the signal near K1 varies from
126 site to site, possibly due to multipath [*Georgiadou and Kleusberg*, 1988]. Amplitudes are
127 typically several millimeters at \sim K1, K2, S1 and S2, although can exceed 10 mm at some
128 sites at these frequencies. This variability shows no obvious geographical correlation or
129 dependence.

130

131 To test the constancy of these signals over the time series, we computed short-time
132 Fourier transforms (spectrograms) for each site and compared these with those produced
133 from simulated time series. The spectrograms used a second-order Goertzel algorithm
134 [*Burrus and Parks*, 1985] approach enabling specific attention to the diurnal and semi-
135 diurnal bands. To generate the simulated time series, firstly a harmonic analysis was
136 performed on the entire time series and then a coordinate time series prediction made
137 based on the determined time-constant (in amplitude and phase) constituent frequencies.
138 The spectrogram was computed for this predicted time series and therefore shows only
139 the effect of the diurnal and semi-diurnal constituents shifting in and out of phase.

140 Through comparison, the spectrograms of the observed time series suggest a time-varying
141 behavior in the semi-diurnal and diurnal frequency bands, with Figure 3 an example for
142 the height component of BAHR. This time-varying behavior will add complexity to any
143 resulting long-period signals since it is not a simple time-constant systematic error as
144 considered in *Penna et al.* [2007].

145

146 The sources of these sub-daily signals can, at present, only be partially explained.
147 Previous analyses have reported biases in K1 and K2 estimates using GPS (see e.g.,
148 *Schenewerk et al.* [2001]) with inadequate satellite orbit modeling and multipath
149 suggested as possible causes. For the S1 and S2 signals, *Tregoning and van Dam* [2005]
150 show atmospheric pressure loading displacements of the order of 0.5-1.5 mm at these
151 frequencies, although these are too small to explain a large portion of the signal observed
152 in our time series. The clear latitude dependent relationship of the S1 and S2 atmospheric
153 loading displacements is also not evidenced in our time series. Residual tropospheric
154 delay errors may contribute to the S1 signals, and higher-order ionospheric effects (not
155 taken in consideration in our analysis) may be partially responsible for the signal in the
156 diurnal frequency band, but its sub-daily characteristic at a wide range of sites is not yet
157 well known [*Fritsche et al.*, 2005]. Residual solid Earth tide and ocean tide loading
158 signals are expected to be typically less than 1-2 mm at these frequencies at the majority
159 of sites [see *Penna et al.*, 2007]. The observed spectra are therefore largely unexplained at
160 present. However, as previously mentioned, their presence in GPS analyses involving
161 conventional 24 h sessions, regardless of their origin, may result in spurious long-period
162 signals at periods of distinct geophysical interest.

163

164 **3.2 Propagation to long periods**

165 In order to assess the effects of these signals on 24 h solutions, the conventional 24 h
166 solution was compared with the high rate analysis. The 24 h coordinate time series were
167 linearly interpolated to 0.5 h and differenced from the time series described in Section
168 3.1. This differencing removes any common geophysical signal and common mode noise.
169 The resultant difference time series then contains unmodeled sub-daily signals (from the
170 0.5 h solutions) and any resulting long-period propagated signals. It is important to note
171 for clarity that *i*) all common long-period (>1 day) geophysical signal is differenced, and
172 *ii*) that sub-daily signals in all three coordinate components propagate into the height
173 coordinate time series [Penna *et al.*, 2007]. The amplitude spectra of these differenced
174 time series were then computed, revealing significant signals with, or close to, annual and
175 semi-annual periods. In some cases, signals were evident also at 1/3 and 1/4 years.
176 Amplitude spectra for a selection of sites are shown in Figure 4.

177

178 Fitting offset, linear rate and annual and semi-annual periodic terms to these differenced
179 time series reveals the level of propagation at each site, as shown in Figure 1. Annual
180 propagated signals reach ~4.2 mm (height), 1.0 mm (north) and 2.4 mm (east), with
181 corresponding median values of 0.8 mm, 0.3 mm and 0.6 mm. Semi-annual propagated
182 signals reach ~3.8 mm (height), 0.9 mm (north) and 5.5 mm (east), with corresponding
183 median values of 0.6 mm, 0.2 mm and 0.4 mm.

184

185 Fitting only annual, semi-annual and linear terms leaves long-period signal (periods
186 longer than ~3 months) in the time series, which we attribute to arise from the time-
187 varying sub-daily signals producing broad spectral peaks. These include the harmonics of

188 one year plus signal just greater than one year which could bias velocity estimates
189 [Blewitt and Lavallée, 2002]. This residual noise contributes to GPS coordinate time
190 series noise at the level of a few millimeters, on average.
191
192 4. Discussion and Conclusions
193 The signal present in these differenced time series would normally be indistinguishable
194 from real geophysical signals of interest in conventional 24 h time series and hence would
195 bias per-site estimates of low frequency geophysical loading and mass transfer signals.
196 Comparing the amplitudes and phases of the semi-annual and annual terms (Figure 1)
197 over western Europe, where the site density is greatest, suggests a level of signal
198 coherence. However, signal coherence is not evident over larger regions (e.g., Australia),
199 where the site density is lower. The level of bias will, therefore, be specific to each
200 chosen study region. .
201
202 Computing their effect on low-degree ($n \leq 4$) spherical harmonic coefficients of non-
203 secular global surface mass loading, reveals that, for this 90-site network, they may bias
204 estimates by up to 5-10%, plus add random noise to their solution. Inferred loading
205 estimates from time periods earlier than those considered here (pre-2000) may be subject
206 to larger site-by-site biases due to worse sub-daily modeling at that time [Watson *et al.*,
207 2006] and greater effects from individual stations due to decreased station density. For
208 example, Blewitt *et al.* [2001], used a cumulative IGS time series that, from 1994 until at
209 least 2004, included insufficient or erroneous sub-daily solid earth tide models and fewer
210 stations than used here. Furthermore, inter-comparison of GPS time series with GRACE

211 data at semi-annual annual periods [e.g., *King et al.*, 2006] will be affected by these
212 errors.

213

214 Different orbit/clock products may also induce different sub-daily errors. Indeed,
215 determining sub-daily solutions on a 15 site subset of the network using IGS products
216 instead of JPL ones produced similar results but, when compared to the JPL spectra, the
217 IGS spectra contained considerably broader peaks at sub-daily frequencies with typically
218 larger amplitudes. Greater levels of site-by-site long-period signal bias would therefore be
219 expected, with consequently larger (systematic and/or random) errors in low degree
220 spherical harmonics derived from them.

221

222 To address the biases we have identified, the source(s) of these unmodeled signals must
223 be determined. Satellite orbit modeling error is perhaps the most likely source of large
224 (>2 mm) signals around K1 and K2 frequencies together with multipath [*Ray et al.*,
225 2007]. Candidate causes of the S1 and S2 signals are residual tropospheric delay and
226 mapping function errors as well as atmospheric pressure loading and higher order
227 ionospheric effects. In the absence of models accurate to ~ 0.1 mm, conventional 24 h
228 ‘static’ solutions are not ideal and alternative parameterizations may need to be
229 considered when analyzing GPS observation data for seasonal atmospheric, hydrologic
230 and oceanic loading studies.

231

232 **Acknowledgements**

233 We thank the IGS community for provision of GPS data, JPL for GIPSY software,
234 satellite orbits and clocks, Duncan Agnew for making SPOTL available and Gary Egbert
235 for making TPXO6.2 available. MAK was supported by a NERC postdoctoral fellowship.

236

237 **References**

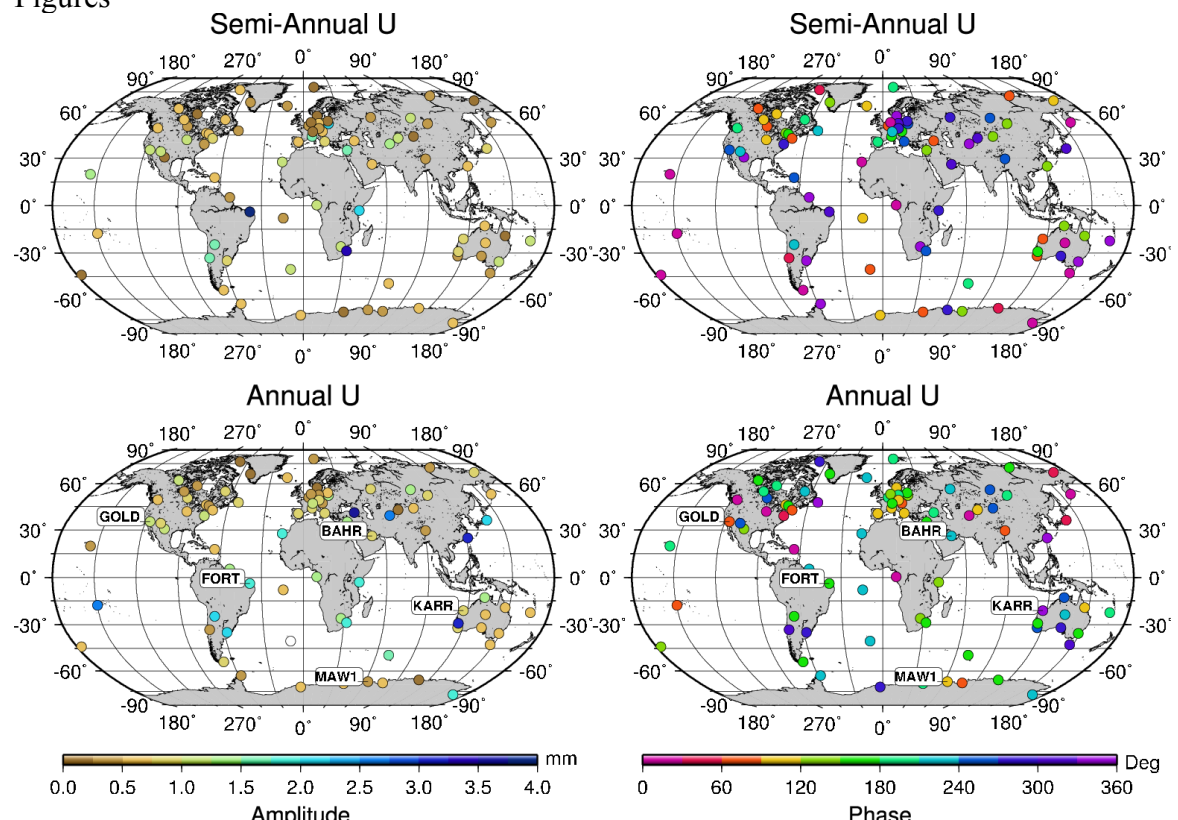
- 238 Agnew, D. C. (1997), NLOADF: A program for computing ocean-tide loading, *J.*
239 *Geophys. Res.*, *102*, 5109-5110.
- 240 Blewitt, G., and D. Lavallée (2002), Effect of annual signals on geodetic velocity, *J.*
241 *Geophys. Res.*, *107*, doi:10.1029/2001JB000570.
- 242 Blewitt, G., D. Lavallée, P. Clarke, and K. Nurutdinov (2001), A New Global Mode of
243 Earth Deformation: Seasonal Cycle Detected, *Science*, *294*, 2342-2345, DOI:
244 2310.1126/science.1065328.
- 245 Burrus, C. S., and T. W. Parks. (1985), *DFT/FFT and Convolution Algorithms*, 232 pp.,
246 John Wiley & Sons, New York, NY.
- 247 Dow, J. M., R. E. Neilan, and G. Gendt (2005), The International GPS Service:
248 Celebrating the 10th anniversary and looking to the next decade, *Advances in Space*
249 *Research*, *36*, 320-326.
- 250 Egbert, G. D., and S. Y. Erofeeva (2002), Efficient inverse modeling of barotropic ocean
251 tides, *J. Atmos. Ocean. Technol.*, *19*, 183-204.
- 252 Fritsche, M., R. Dietrich, C. Knofel, A. Rulke, S. Vey, M. Rothacher, and P.
253 Steigenberger (2005), Impact of higher-order ionospheric terms on GPS estimates,
254 *Geophys. Res. Lett.*, *32*, L23311, doi:2310.21029/22005GL024342.
- 255 Georgiadou, Y., and A. Kleusberg (1988), On carrier signal multipath effects in relative
256 GPS positioning, *Manuscr. Geodaet.*, *13*, 172-179.
- 257 Humphreys, T. E., M. C. Kelley, N. Huber, and P. M. Kintner (2005), The semidiurnal
258 variation in GPS-derived zenith neutral delay, *Geophys. Res. Lett.*, *32*, L24801,
259 doi:24810.21029/22005GL024207.

- 260 Khan, S. A., and H. G. Scherneck (2003), The M₂ ocean tide loading wave in Alaska:
261 vertical and horizontal displacements, modelled and observed, *J. Geodesy*, 77, 117-
262 127, doi: 110.1007/s00190-00003-00312-y.
- 263 King, M. (2006), Kinematic and static GPS techniques for estimating tidal displacements
264 with application to Antarctica, *J. Geodyn.*, 41, 77-86,
265 doi:10.1016/j.jog.2005.1008.1019.
- 266 King, M., and S. Aoki (2003), Tidal observations on floating ice using a single GPS
267 receiver, *Geophys. Res. Lett.*, 30, 1138 doi:1110.1029/2002GL016182.
- 268 King, M., R. Coleman, and L. Nguyen (2003), Spurious periodic horizontal signals in
269 sub-daily GPS position estimates, *J. Geodesy*, 77, 15-21, doi:10.1007/s00190-00002-
270 00308-z.
- 271 King, M. A., P. Moore, P. J. Clarke, and D. L. Lavallée (2006), Choice of optimal
272 averaging radii for temporal GRACE gravity solutions, a comparison with GPS and
273 satellite altimetry, *Geophys. J. Int.*, 166, 1-11, doi: 10.1111/j.1365-
274 1246X.2006.03017.x.
- 275 Mangiarotti, S., A. Cazenave, L. Souderin, and J. F. Cretaux (2001), Annual vertical
276 crustal motions predicted from surface mass redistribution and observed by space
277 geodesy, *J. Geophys. Res.*, 106, 4277-4291.
- 278 McCarthy, D. D., and G. Petit (2004), IERS Conventions (2003), IERS Technical Note,
279 127 pp, Frankfurt am Main: Verlag des Bundesamts für Kartographie und Geodäsie.
- 280 Penna, N. T., M. A. King, and M. P. Stewart (2007), GPS height time series: Short period
281 origins of spurious long period signals, *J. Geophys. Res.*, 112, B02402,
282 doi:02410.01029/02005JB004047.

- 283 Penna, N. T., and M. P. Stewart (2003), Aliased tidal signatures in continuous GPS height
284 time series, *Geophys. Res. Lett.*, *30*, 2184, doi:2110.1029/2003GL018828.
- 285 Press, W. H., S. A. Teukolsky, W. T. Vetterling, and F. B.P. (1992), *Numerical Recipes in*
286 *FORTRAN 77: The Art of Scientific Computing*, 2nd ed., Cambridge University Press,
287 New York.
- 288 Ray, J., Z. Altamimi, X. Collilieux, and T. Van Dam (2007), Anomalous harmonics in the
289 spectra of GPS position estimates, *GPS Sol.*, doi:10.1007/s10291-007-0067-7.
- 290 Rothacher, M., G. Beutler, R. Weber, and J. Hefty (2001), High-frequency variations in
291 Earth rotation from Global Positioning System data, *J. Geophys. Res.*, *106*, 13711-
292 13738.
- 293 Scargle, J. D. (1982), Studies in astronomical time series analysis. II. Statistical aspects of
294 spectral analysis of unevenly spaced data, *Astronomical Journal*, *263*, 835-853.
- 295 Schenewerk, M. S., J. Marshall, and W. Dillinger (2001), Vertical ocean-loading
296 deformations derived from a global GPS network, *J. Geod. Soc. Japan*, *47*, 237-242.
- 297 Stewart, M. P., N. T. Penna, and D. D. Lichti (2005), Investigating the propagation
298 mechanism of unmodelled systematic errors on coordinate time series estimated using
299 least squares, *J. Geodesy*, *79*, 479-489, doi:410.1007/s00190-00005-00478-00196.
- 300 Tregoning, P., and T. van Dam (2005), Atmospheric pressure loading corrections applied
301 to GPS data at the observation level, *Geophys. Res. Lett.*, *32*, L22310,
302 doi:22310.21029/22005GL024104.
- 303 van Dam, T., J. Wahr, and D. Lavallée (2007), A comparison of annual vertical crustal
304 displacements from GPS and Gravity Recovery and Climate Experiment (GRACE)
305 over Europe, *J. Geophys. Res.*, *112*, B03404, doi:03410.01029/02006JB004335.

- 306 van Dam, T. M., and J. Wahr (1998), Modeling Environment Loading Effects: a Review,
307 *Phys. Chem. Earth*, 23, 1077-1087.
- 308 Watson, C., P. Tregoning, and R. Coleman (2006), The impact of solid earth tide models
309 on GPS coordinate and tropospheric time series, *Geophys. Res. Lett.*, 33, L08306,
310 doi:10.1029/2005GL025538.
- 311 Wu, X. P., M. B. Heflin, E. R. Ivins, D. F. Argus, and F. H. Webb (2003), Large-scale
312 global surface mass variations inferred from GPS measurements of load-induced
313 deformation, *Geophys. Res. Lett.*, 30, 1742, doi:10.1029/2003GL017546.
- 314 Zumberge, J. F., M. B. Heflin, D. C. Jefferson, M. M. Watkins, and F. H. Webb (1997),
315 Precise point positioning for the efficient and robust analysis of GPS data from large
316 networks, *J. Geophys. Res.*, 102, 5005-5017.
- 317
- 318

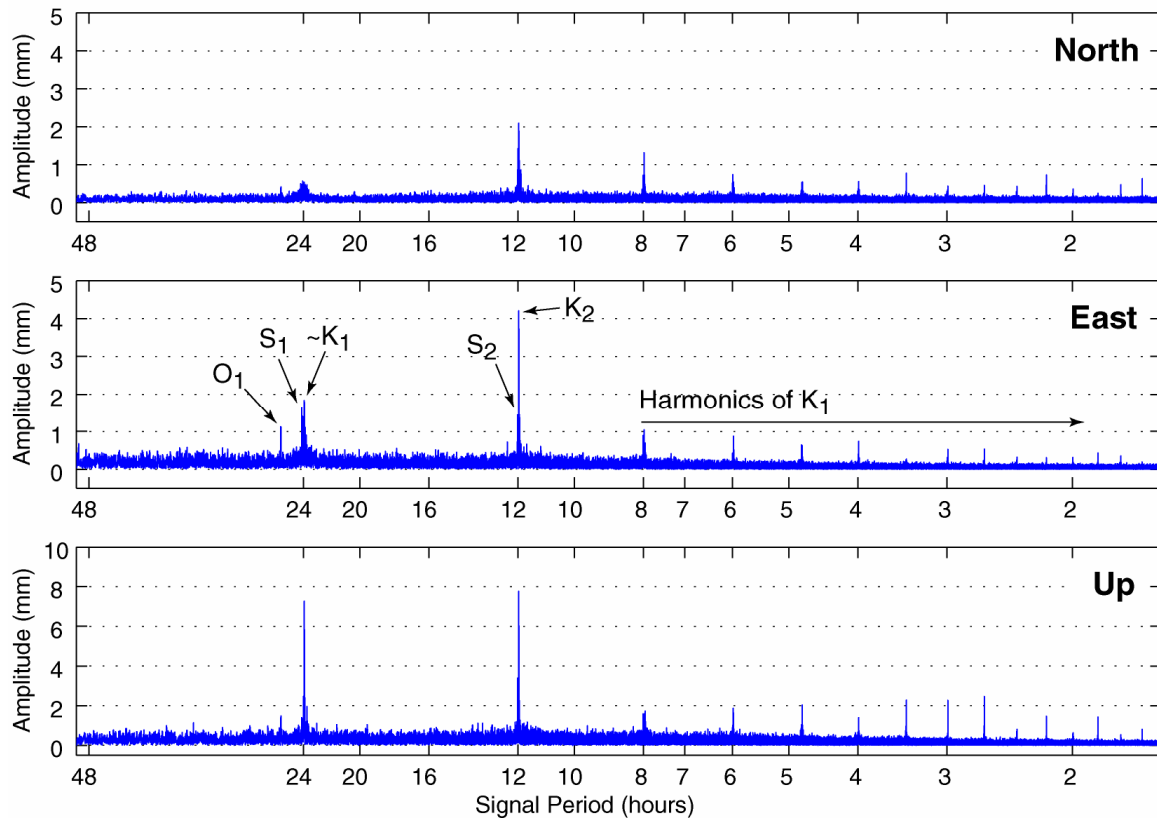
319 Figures



320

321 Figure 1: Height component semi-annual (top) and annual (bottom) amplitudes (left) and
322 phases (right) due to the propagation of unmodelled sub-daily signals.

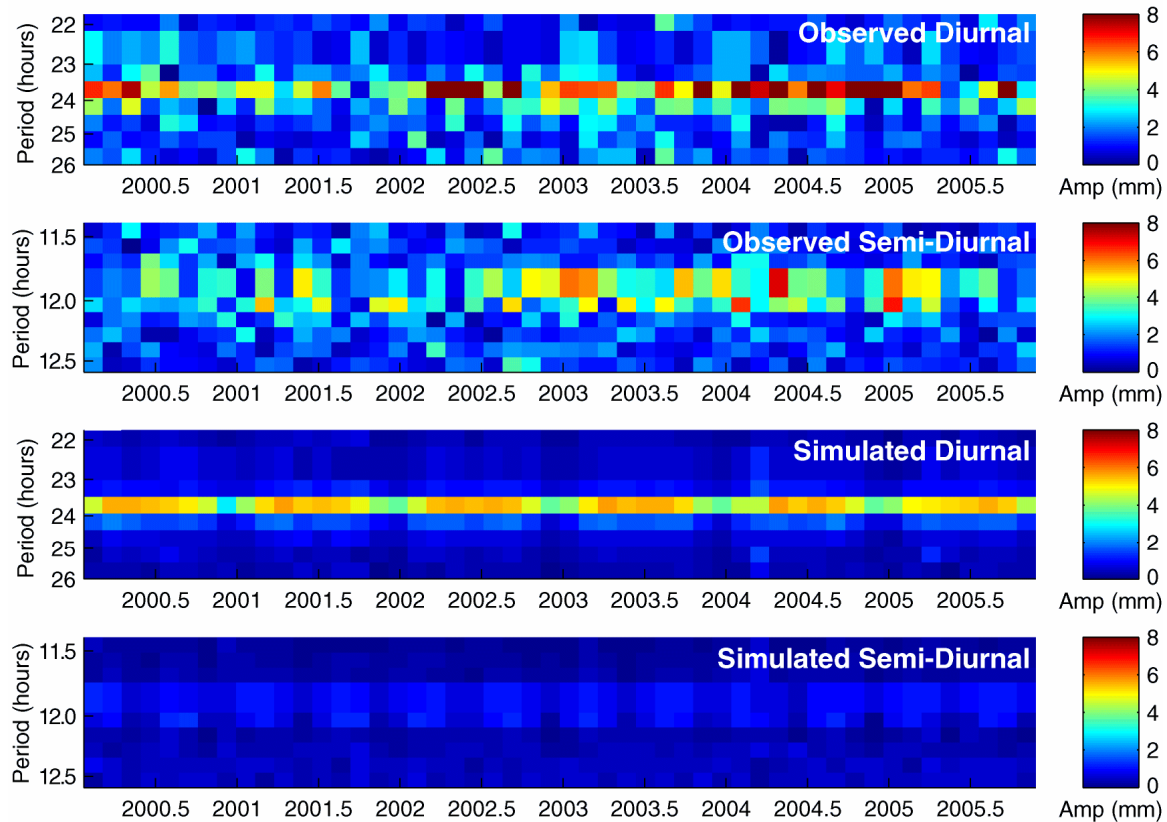
323



324

325 Figure 2: Spectra of the GOLD coordinate time series generated from the sub-daily PPP
326 time series.

327



328

329

330 Figure 3: Spectrogram for the height component of site BAHR in the diurnal and semi-
331 diurnal frequency bands using the observed time series and a simulated time series for
332 BAHR based on assumed time-constancy of each constituent.

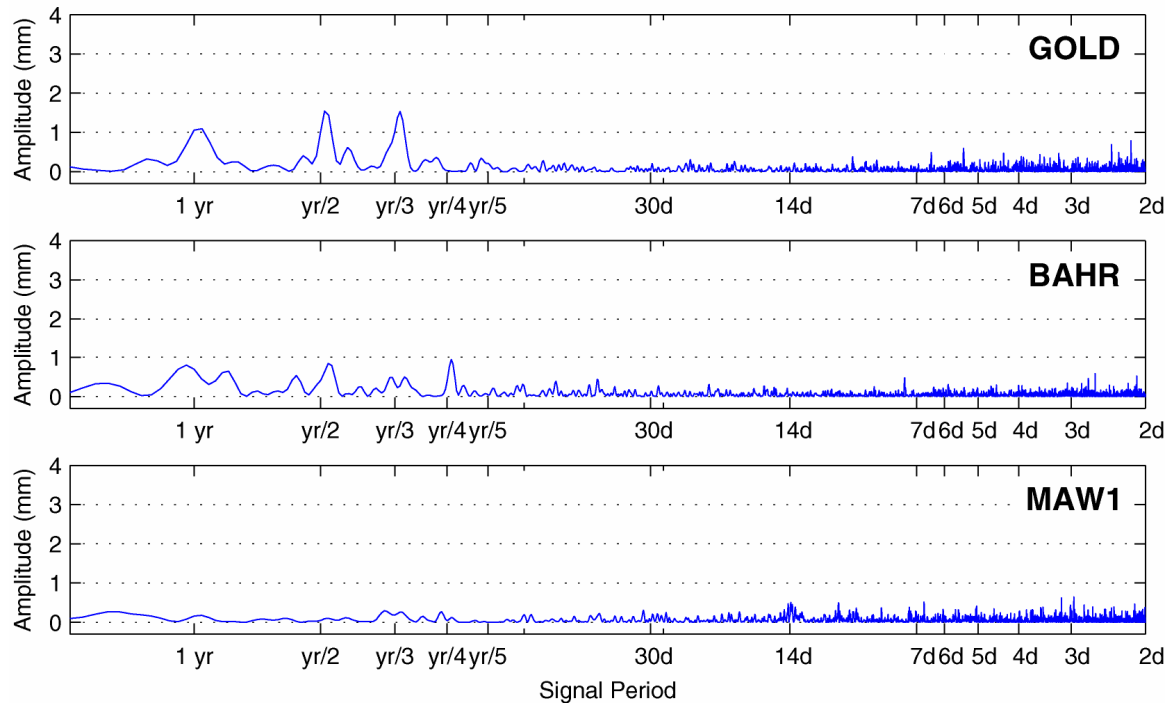
333

334

335

336

337



338

339

340 Figure 4: Long-period spectra of the differences between the 24 h and sub-daily PPP
341 solutions for GOLD, BAHR and MAW1, arising from the propagation of unmodeled sub-
342 daily signals.

343

344

345